Structural Features of Distinctin Affecting Peptide Biological and Biochemical Properties[†]

Mauro Dalla Serra,[‡,§] Oscar Cirioni,[§,||] Rosa Maria Vitale,[§,⊥] Giovanni Renzone,[§,#] Manuela Coraiola,[‡] Andrea Giacometti,[||] Cristina Potrich,[‡] Elisa Baroni,[‡] Graziano Guella,[‡,+] Marina Sanseverino,[▽] Stefania De Luca,[@] Giorgio Scalise,[||] Pietro Amodeo,[⊥] and Andrea Scaloni*[,#]

Bruno Kessler Foundation, Institute of Biophysics, National Research Council, 38100 Povo (Trento), Italy, Institute of Infectious Diseases and Public Health, Polytechnic Marche University, 60200 Ancona, Italy, Institute of Biomolecular Chemistry, National Research Council, 80078 Pozzuoli (Naples), Italy, Proteomics and Mass Spectrometry Laboratory, ISPAAM, National Research Council, 80147 Naples, Italy, Laboratory of Bioorganic Chemistry, Department of Physics, University of Trento, 38100 Povo (Trento), Italy, Inbios S.r.l., 80078 Pozzuoli (Naples), Italy, and Institute of Biostructures and Bioimages, National Research Council, 80138 Naples, Italy

Received April 8, 2008; Revised Manuscript Received May 27, 2008

ABSTRACT: The antimicrobial peptide distinctin consists of two peptide chains linked by a disulfide bridge; it presents a peculiar fold in water resulting from noncovalent dimerization of two heterodimeric molecules. To investigate the contribution of each peptide chain and the S−S bond to distinctin biochemical properties, different monomeric and homodimeric peptide analogues were synthesized and comparatively evaluated with respect to the native molecule. Our experiments demonstrate that the simultaneous occurrence of both peptide chains and the disulfide bond is essential for the formation of the quaternary structure of distinctin in aqueous media, able to resist protease action. In contrast, distinctin and monomeric and homodimeric analogues exhibited comparable antimicrobial activities, suggesting only a partial contribution of the S−S bond to peptide killing effectiveness. Relative bactericidal properties paralleled liposome permeabilization results, definitively demonstrating that microbial membranes are the main target of distinctin activity. Various biophysical experiments performed in membrane-mimicking media, before and after peptide addition, provided information about peptide secondary structure, lipid bilayer organization, and lipid−peptide orientation with respect to membrane surface. These data were instrumental in the generation of putative models of peptide−lipid supramolecular pore complexes.

Amphibian skin granular glands are a rich source of bioactive compounds, and a large number of antimicrobial peptides in their secreted fluids have been characterized (*1*). These molecules are recognized as essential components of animal innate defense systems (*2, 3*). Although greatly diverse in primary structure, these peptides have been grouped into three broad families on the basis of their sequence and structural characteristics (*1, 2*). The first one includes a large group of linear amphipathic peptides, such as magainins, bombinins, dermaseptins, caerins, and temporins (*1, 2*). The second family includes peptides (ranalexins, brevinins, japonicins, gaegurins, and esculentins) containing two Cys residues at the C-terminus linked by a disulfide bridge forming a seven- to nine-amino acid cyclic moiety (*1, 2*). Members of both classes present an unstructured design in water but adopt an amphipathic helical conformation in hydrophobic media (*4–8*). The third family includes uncommon molecules consisting of two peptide chains linked by a disulfide bond, as in the case of the heterodimeric polypeptide distinctin from *Phyllomedusa distincta* (Figure 1) (*9*). Distinctin-related hetero- and homodimeric peptides with bactericidal properties, namely, dicynthaurin, halocidin, and cathelicidins CAP11 and PMAP36, have also been reported in hemocytes of *Halocynthia aurantium* or guinea pig neutrophils (*10–13*). No sequence homology was detected between these molecules. Conformational studies demonstrated also for these peptides the intrinsic tendency to adopt an amphipatic helical structure in a membrane-mimicking environment (*9, 10, 13–16*), well exemplified by the helical wheel diagram of the distinctin chains (Figure 1).

Members of all peptide classes have shown a broad spectrum of antimicrobial activity, presenting a remarkable range of action on Gram-positive and -negative bacteria, yeast, fungal strains, and protozoa (*1–3, 17, 18*). It was

[†] This work was partially supported by grants from the Italian National Research Council (AG.P04.015 and RSTL 862), by Provincia Autonoma di Trento (Project SyrTox), and by structural funds from the Italian National Research Council and the Bruno Kessler Foundation.

* To whom correspondence should be addressed: Proteomics and Mass Spectrometry Laboratory, ISPAAM, National Research Council, via Argine 1085, I-80147 Napoli, Italy. Telephone: ++39-081-5966006. Fax: ++39-081-5965291. E-mail: andrea.scaloni@ispaam.cnr.it.

[‡] Institute of Biophysics, National Research Council.

[§] These authors contributed equally to this work.

[||] Polytechnic Marche University.

[⊥] Institute of Biomolecular Chemistry, National Research Council.

[#] ISPAAM, National Research Council.

[+] University of Trento.

[▽] Inbios S.r.l.

[@] Institute of Biostructures and Bioimages, National Research Council.

10.1021/bi800616k CCC: $40.75
Published on Web 07/03/2008

Peptide	Structure
Distinctin	ENREVPPGFTALIKTLRKCKII NLVSGLIEARKYLEQLHRKLKNCKV
Peptide A	ENREVPPGFTALIKTLRKCKII
Peptide A-A homodimer	ENREVPPGFTALIKTLRKCKII ENREVPPGFTALIKTLRKCKII
Peptide B	NLVSGLIEARKYLEQLHRKLKNCKV
Peptide B-B homodimer	NLVSGLIEARKYLEQLHRKLKNCKV NLVSGLIEARKYLEQLHRKLKNCKV

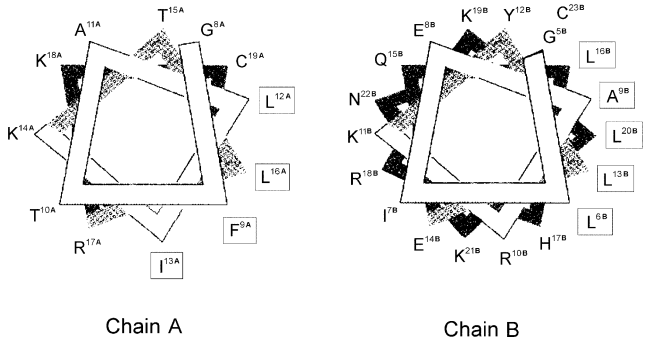

FIGURE 1: Structures of distinctin and peptide analogues used in this study (top panel) and helical wheel diagrams of the distinctin peptide chains (bottom panel). The clearly evident clustering of polar and apolar residues imparts amphipathicity.

also demonstrated that some compounds exhibit other important properties, such as antitumor, spermicidal, and anti-HIV activities (*19–21*). The detailed molecular mechanism of their antimicrobial action and selectivity has not been definitively clarified. Most antimicrobial peptides are cationic and interact with negatively charged phospholipids, which are characteristic components of most target microbes. The Shai−Mausuzaki−Huang model was generally regarded as the most reliable molecular hypothesis for explaining their antimicrobial action (*22–24*).

In the past, we have focused our attention on the biochemical and structural properties of distinctin (*9, 16*). Nuclear magnetic resonance (NMR) studies revealed the peculiar conformation of the distinctin noncovalent dimer in aqueous solution, characterized by a symmetrical full-parallel four-helix bundle with a well-secluded hydrophobic core and exposed basic residues (*16*). This structure demonstrated that dimerization of a heterodimeric peptide can yield an uncommon transport form, more compact and resistant to proteases than that observed for the linear amphipathic molecules (*16*). This unique fold significantly stabilizes distinctin structure without affecting its potential to form ion channels in synthetic membranes. Since distinctin presents various structural moieties, i.e., two distinct polypeptide chains and an interchain disulfide bond, which may determine its peculiar biochemical characteristics, we synthesized various peptide analogues that were assayed in comparison to highlight the molecular features essential for the functioning of the native peptide.

EXPERIMENTAL PROCEDURES

Materials. Reagents for peptide synthesis were purchased from Novabiochem. Polymyxin B was from Sigma-Aldrich; HPLC-grade solvents were from Riedel-de Haen (Seelze, Germany). Lipids were purchased from Avanti Polar Lipids (Alabaster, AL).

Peptide Synthesis. Peptide chains were synthesized by 9-fluorenyl-methoxycarbonyl solid phase chemistry (*16*). Homo- and heterodimer peptides were obtained by a dropwise addition of a solution containing a single peptide chain in 0.1 M NH_4HCO_3 to the other peptide chain dissolved in the same buffer. Disulfide bond formation was achieved simply by air oxidation at room temperature in 48−72 h. All peptides were purified by preparative reversed phase HPLC and characterized as pure components by analytical reversed phase HPLC and MALDI-TOF MS analysis: distinctin, measured mass of 5478.9 Da (theoretical mass, 5478.6 Da); peptide A, measured mass of 2527.1 Da (theoretical mass, 2527.4 Da); peptide B, measured mass of 2953.6 Da (theoretical mass, 2953.2 Da); peptide A−A homodimer, measured mass of 5053.3 Da (theoretical mass, 5052.8 Da); and peptide B−B homodimer, measured mass of 5905.5 Da (theoretical mass, 5905.1 Da).

Size Exclusion Chromatography. Size exclusion chromatography of distinctin analogues was carried out as previously reported (*16*).

Proteolysis Experiments. Comparative proteolysis experiments with melittin and distinctin analogues were performed in parallel, incubating isolated peptides (300 pmol) in 50 mM ammonium acetate at pH 6.5 and 37 °C with equal amounts of trypsin, chymotrypsin, or elastase. Added enzyme amounts ranged from 15 to 0.1 ng. Digestion aliquots (30 pmol) were withdrawn on a time course basis and directly analyzed with a Voyager-DE PRO MALDI-TOF spectrometer (Applera) as previously reported (*16*).

MIC, MBC, and Cytotoxicity Assays. A total of 101 nonduplicate clinical isolates were tested and consisted of methicillin-resistant *Staphylococcus aureus* (10 isolates), methicillin-susceptible *S. aureus* (10 isolates), *Streptococcus pneumoniae* (10 isolates), *Enterococcus faecium* (5 isolates), *Enterococcus faecalis* (10 isolates), *Acinetobacter baumannii* (8 isolates), *Pseudomonas aeruginosa* (10 isolates), *Stenotrophomonas maltophilia* (8 isolates), *Klebsiella pneumoniae* (10 isolates), *Serratia marcescens* (10 isolates), and *Escherichia coli* (10 isolates). Antimicrobial compounds were made fresh on the day of assay or stored at −80 °C in the dark, for a maximum of 2 weeks. MICs were assayed at 5×10^5 CFU/mL on Mueller-Hinton (MH) broth by the microbroth dilution method, according to the procedures outlined by the Clinical and Laboratory Standards Institute (*25*). Polypropylene 96-well plates (Sigma-Aldrich) were incubated for 18 h at 37 °C, in air, and gently shaken throughout the study. The MIC was taken as the lowest drug concentration at which observable growth was inhibited. The MBC was taken as the lowest concentration of each drug that resulted in a >99.9% reduction of the initial inoculum. Experiments were performed in triplicate.

A-549 cells from human lung carcinoma (BioWhittaker Inc., Walkersville, MD) were cultured in 25 cm^2 flasks, using DMEM with 10% fetal calf serum (BioWhittaker) as the culture medium. The cytotoxicity of distinctin at 1× MBC was determined by the CellTiter 96 AQ cell proliferation assay (Promega, Lyon, France).

Calcein Release Assays. Large unilamellar vesicles (LUVs)[1] loaded with a self-quenching concentration of calcein (80 mM) were prepared by extrusion through two stacked polycarbonate filters with 100 nm pores (*26, 27*). Prepared vesicles were monodispersed with a diameter in the range of 117−130 nm, as measured by dynamic light scattering (*27, 28*). Nonencapsulated calcein was removed by spinning the LUV suspension through a Sephadex G50 minicolumn (Sigma). Lipid mixture ratios reported in the text are given on an equimolar molar basis. Peptide permeabilization activity was obtained by fluorescence measurements (*27*). Aliquots of washed LUVs were introduced into 200 μL of 140 mM NaCl, 20 mM Hepes, and 1 mM EDTA (pH 7.0) to produce a final lipid concentration of 6−8 μM. The percent of permeabilization ($R_{\%}$) was then calculated as $(F_{fin} - F_{in})/(F_{max} - F_{in}) \times 100$, where F_{in} and F_{fin} represent the initial and final values of fluorescence before and after peptide addition, respectively. F_{max} is the maximum calcein release and was obtained by adding 1 mM Triton X-100. Unspecific binding to plastic walls was reduced by pretreating the microplate with a 0.1 mg/mL Prionex solution. The spontaneous leakage of calcein from LUVs was negligible.

Fourier Transform Infrared Spectroscopy Experiments. Attenuated total reflection Fourier transform infrared spectroscopy (ATR-FTIR) was used to investigate changes in secondary structure when peptide passes from the aqueous phase to the lipid phase (*27, 29*). Lyophilized peptides were suspended in 10 mM Hepes (pH 7.4); to prevent undesired oxidation, peptide A and B solutions also contained 20 mM DTT. For spectroscopic measurements, a drop of sample was spread on 10-reflection Ge crystals (45° cut) and gently dried under N_2 flushing. For measurements in the lipid phase, peptides in 10 mM Hepes (pH 7.4) were incubated for 1 h, at 25 °C, with LUVs made of 1-palmitoyl-2-oleoyl-*sn*-glycero-3-phosphocholine (POPC) and 1,2-dioleoyl-*sn*-glycero-3-phosphate (DOPA) in a 1:1 molar ratio. LUVs were prepared as described above, except that dried lipids were hydrated in 10 mM Hepes (pH 7.4) without calcein. The lipid-to-peptide ratio (L:P) used was set to favor the maximum formation of active pores in the membrane, i.e., the L:P able to cause 90% activity according to an equivalent assay of calcein release. Thus, L:P values of 50 and 25 were used for distinctin and peptide homodimers. Due to their weaker ability to bind LUVs, a L:P of 50 was used for peptide A and B, which corresponded to <20% of activity in the calcein release assay. After incubation, aqueous/LUV mixtures were centrifuged at 350000*g*, for 3 h, at 4 °C. The pellet was suspended in 100 μL of 10 mM Hepes (pH 7.4) and directly deposited on Ge crystals. Spectra of hydrated and deuterated films were collected, in ATR geometry, using a FTS 185 spectrometer (Bio-Rad), with an MCT detector. For the polarization experiments, a rotating KRS5 wire-grid polarizer was interposed and set at either 0° or 90° (with respect to the plane of internal reflections). The orientation of a structural element was calculated from the dichroic ratio $R = A_{0°}/A_{90°}$, where $A_{0°}$ and $A_{90°}$ are the absorption bands pertaining to the functional group of that element, in parallel and perpendicular configurations, respectively (*30*). For the sake of simplicity, we considered in most of the cases the absorption intensity of the spectra at 0° and 90°, at the frequency typical of that structural element. By using *R*, we calculated form factor *S*, which was then used to calculate average tilt angle γ (*29*).

To estimate the secondary structure content, the amide I′ band in the region of 1700−1600 cm^{-1} was deconvolved into a set of Lorentzian components whose frequencies were assigned to different structural elements (*27, 31*). Two additional bands around 1624 and 1692 cm^{-1} were observed for peptide A, which are typical of aggregated peptides in an extended configuration (*32*). That set of Lorentzians was used to best fit the original spectrum, and the resulting relative areas were taken as the proportion of the related structure present. A small side chain band and bands from the aggregated state were excluded from normalization. In the case of lipid-bound peptide, the spectrum of the peptide was obtained after subtracting the contribution of the lipid alone, with a weight that minimized the band at 1738 cm^{-1}, as a result of the high L:P values that were used. To calculate the lipid contribution in the methylene C−H stretching region (from 3000 to 2800 cm^{-1}), a subtraction of the peptide spectrum from the lipid−peptide one was performed. In the pellet, the L:P value was calculated by the following algorithm (*29*):

$$\text{L:P} = 0.208(n_{res} - 1)\frac{(1 - S_{\text{amide I}'})\int_{2800}^{2980} A_{90°}(\nu_L)\,d\nu}{(1 - S_L/2)\int_{2800}^{2980} A_{90°}(\nu_{\text{amide I}'})\,d\nu} \quad (1)$$

where n_{res} is the number of residues of the peptide, $A_{90°}$ is the absorption with the polarizer set at 90°, and S_L and $S_{\text{amide I}'}$ are order parameters calculated from the ratio of the parallel and perpendicular absorption bands, respectively (*29, 30*). In particular, S_L is for the lipid chains, derived from the symmetric and asymmetric methylene C−H stretching (bands centered at 2853 and 2923 cm^{-1}, respectively) using θ set at 90°; $S_{\text{amide I}'}$ is the order parameter for the amide I′ band (with $\theta = 0°$). The integrals with suffixes L and amide I′ were calculated from the spectrum of the lipid alone and that of the peptide, respectively.

NMR Experiments. ^{31}P NMR spectra of 1:1 POPC/DOPA mixtures before and after addition of distinctin were recorded and analyzed as described in the Supporting Information.

Molecular Modeling. Models of distinctin pores in aqueous lipid bilayers (1:1 POPC/DOPA) were built up as described in the Supporting Information.

RESULTS

Synthesis of Distinctin Analogues and Their Oligomerization in Aqueous Buffer. With the aim of examining the contribution of each peptide chain, of the disulfide-dependent heterodimerization, and of noncovalent oligomerization on

[1] Abbreviations: ATR, attenuated total reflection; Ch, cholesterol; γ, tilt angle; CSA, chemical shift anisotropy; DOPA, 1,2-dioleoyl-*sn*-glycero-3-phosphate; DOPE, 1,2-dioleoylphosphatidylethanolamine; DOPG, 1,2-dioleoylphosphatidylglycerol; DTT, dithiothreitol; FTIR, Fourier transform infrared; L:P, lipid-to-peptide ratio; LUVs, large unilamellar vesicles; MLVs, multilamellar vesicles; PI, phosphatidylinositol; POPC, 1-palmitoyl-2-oleoyl-*sn*-glycero-3-phosphocholine; PS, phosphatidylserine; *R*, dichroic ratio; *S*, form factor; SM, sphingomyelin; TFA, trifluoroacetic acid.

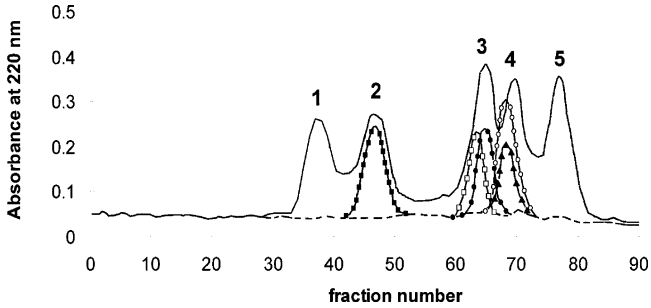

FIGURE 2: Oligomerization properties of distinctin and peptide analogues. Determination of molecular masses by gel filtration chromatography at pH 6.8 of distinctin (■), peptide A (▲), peptide B (○), peptide A−A homodimer (●), and peptide B−B homodimer (□). Elution profiles for chymotrypsinogen (peak 1, 24 kDa), cytochrome (peak 2, 13 kDa), insulin (peak 3, 5.8 kDa), bacitracin (peak 4, 1.4 kDa), and 3-(trimethylsilyl)[2,2,3,3-$^2H_4$]propionate (peak 5, 172 Da) are also reported. A very similar trace was obtained at pH 5.8 (data not shown). The figure summarizes chromatographic runs performed injecting single peptide components or mixtures.

distinctin properties, native molecule and different peptide analogues were prepared. Thus, peptide A, peptide B, peptide A−A homodimer, peptide B−B homodimer, and distinctin (Figure 1) were synthesized, verifying their molecular identity and homogeneity by reversed phase HPLC and MALDI-TOF MS analysis.

To investigate the occurrence of noncovalent interactions between peptide chains, yielding the four-helix bundle structure reported for distinctin in aqueous buffer (*16*), peptide analogues and distinctin were subjected in comparison to size exclusion chromatography experiments, at different pH values. The resulting chromatographic profiles demonstrated that only distinctin exhibited retention times compatible with a dimeric structure (Figure 2). In contrast, peptide monomers and homodimers exhibited elution times close to that of bacitracin (1.4 kDa) or insulin (5.8 kDa), indicative of molecular species occurring as monomeric forms.

Degradation Experiments in Aqueous Buffer. Proteolysis experiments have found wide application in the study of degradation of bioactive polypeptides by proteases as well as in the identification of folded regions in their structures (*33*). Thus, comparative time course proteolysis experiments with distinctin and distinctin analogues were performed; melittin was also analyzed as a peptide having an unfolded structure in aqueous solution. Figure 3 illustrates the different susceptibilities of distinctin to elastase degradation with respect to peptide monomers and homodimers. In contrast to distinctin and like melittin (data not shown), all distinctin analogues were completely degraded after being digested for 6 h. Similar results were obtained during proteolysis with trypsin or chymotrypsin (data not shown). These experiments demonstrated that, although they contain individual molecular moieties present in distinctin structure (i.e., single peptide chains and/or disulfide-linked peptide chains), all distinctin analogues do not simultaneously contain these structural elements, which seem essential for assembly of the folded structure observed for distinctin (*16*), solid enough to resist the action of proteases.

Antimicrobial and Cytotoxic Activity. Distinctin and distinctin analogues exhibited a broad spectrum of antibiotic activity; measured inhibitory effects were comparable for all clinical isolates. Nevertheless, distinctin and peptide A−A and B−B homodimers demonstrated the highest activity against Gram-positive and -negative organisms (Tables 1 and 2). In general, both monomers and dimers were active against antibiotic-resistant organisms, such as MR *S. aureus*, *E. faecalis*, and *S. marcescens*, with the only exception being *P. aeruginosa*, which demonstrated MIC_{50} and MIC_{90} values 2−4-fold higher than those of other bacteria. Among Gram-negative organisms, *E. coli* and *K. pneumoniae* were more susceptible to all compounds. In particular, distinctin and peptide B−B homodimer inhibited their growth at concentrations of 5.84 and 5.42 μM, respectively. On the other hand, *S. maltophilia* and *A. baumannii* were not inhibited and *P. aeruginosa* appeared less susceptible (distinctin and B−B homodimer MIC ranges of 2.92−46.73 and 5.42−43.35, respectively). Measured activities were not comparable to that of polymixin B. For Gram-positive organisms, distinctin and peptide B−B homodimer exerted a similar activity against staphylococci and streptococci; they inhibited their growth at concentrations of 5.84 and 5.42 μM, respectively. In contrast, both *E. faecalis* and *E. faecium* were less susceptible.

The cytotoxic effect was practically absent for all compounds at the concentration that was tested; in fact, measured cytotoxicity on A-549 human lung carcinoma cells was 6.1, 5.6, 5.7, 3.5, and 3.7% for distinctin, peptide A−A homodimer, peptide B−B homodimer, peptide A, and peptide B, respectively.

Liposome Permeabilization. All peptides were able to permeabilize simple model membranes comprised of pure lipids or their mixtures. In fact, they all induced leakage of calcein encapsulated into liposomes. The extent of permeabilization was dependent on peptide type and concentration as well as on composition of lipid vesicles. C_{50} values for vesicle permeabilization are reported in Table 3; they derived from dose dependence experiments similar to those reported in Figure 4. Differences were observed depending on the peptide that was tested and LUV composition; the presence of a negatively charged lipid, i.e., PI, PS, DOPG, or DOPA, was essential for permeabilization activity. This fact is quite common among antimicrobial peptides (*3, 34*), where electrostatic interactions with the target membranes are the first steps leading to their antimicrobial effect. The poor activity measured on LUVs comprised only of POPC, the main phospholipid component of natural membranes, or POPC in a mixture with cholesterol and sphingomyelin, other lipids present in eukaryotic cell membranes, was in good agreement with the high voltages necessary to incorporate distinctin into planar POPC bilayers by repetitive voltage ramps (*16*). On the other hand, comparative experiments with various distinctin analogues demonstrated that distinctin and peptide homodimers exhibited similar activities against liposomes and resulted in compounds being slightly more active than monomeric peptides. These data were in good agreement with MIC_{50} and MIC_{90} measurements. Liposomes did not change their dimension or concentration during the permeabilization process, as checked by dynamic light scattering experiments (data not shown), thus confirming previous evidence of the ability of distinctin to form pores within membranes, rather than exhibiting a detergent-like activity.

FTIR Spectroscopy Experiments. ATR-FTIR spectroscopy was used to investigate the secondary structure of polypeptide

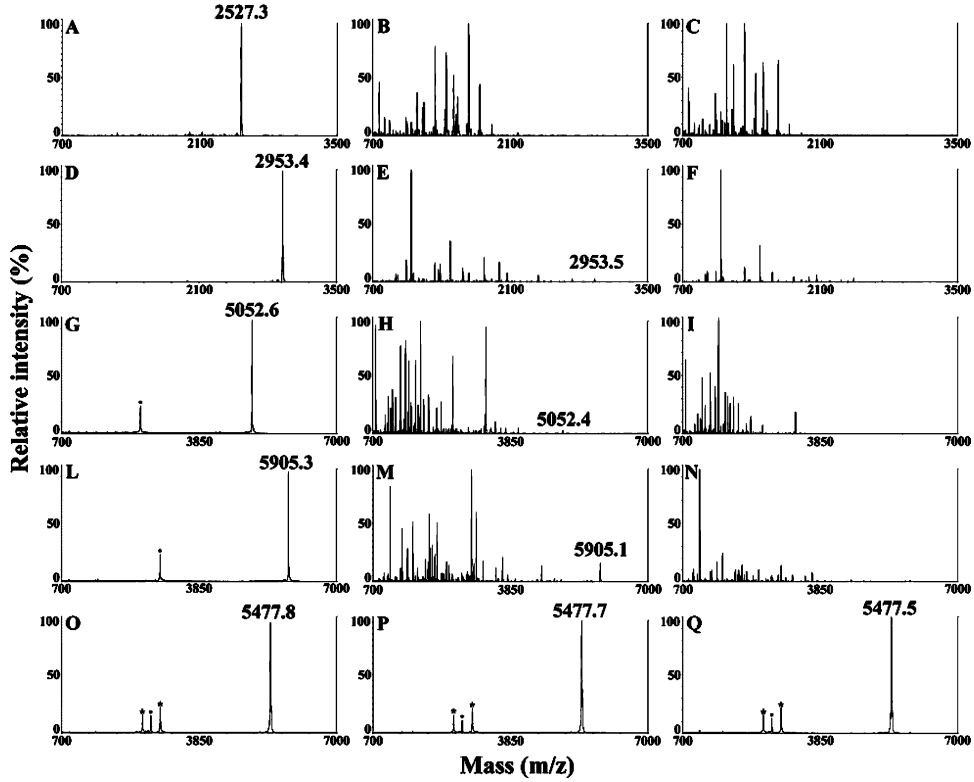

FIGURE 3: Comparative proteolytic degradation of distinctin and peptide analogues. Distinctin, peptide A, peptide B, peptide A−A homodimer, and peptide B−B homodimer (300 pmol) were incubated with 1 ng of elastase in 50 mM ammonium acetate (pH 6.5) at 37 °C. Aliquots (30 pmol) were withdrawn on a time course basis and directly analyzed by MALDI-TOF MS. (A−C) Peptide A after being digested for 0, 3, and 6 h, respectively. (D−F) Peptide B after being digested for 0, 3, and 6 h, respectively. (G−I) Peptide A−A homodimer after being digested for 0, 3, and 6 h, respectively. (L−N) Peptide B−B homodimer after being digested for 0, 3, and 6 h, respectively. (O−Q) Distinctin after being digested for 0, 3, and 6 h, respectively. Filled circles and asterisks indicate doubly charged ions and molecular ions resulting from MALDI in source reduction, respectively. The absence of reduced peptides in distinctin-, peptide A−A homodimer-, and peptide B−B homodimer-containing samples was verified by electrospray mass spectrometry analysis.

chains by analyzing the amide I′ band characteristics (*27, 29*). Absorption spectra were recorded for all the peptides either as pure components or cosedimented with 1:1 POPC/DOPA LUVs. Their secondary structure was estimated by deconvolution and curve fitting with a set of Lorentzian components, which were attributed to different structural elements (Figure 1 of the Supporting Information and Table 4). Frequency component analysis indicated that all peptides in aqueous solution assumed predominantly a helical conformation with the relative secondary structure content in the following order: A−B > B−B = B > A > A−A. Molecular aggregates were observed for peptide A, which may have been occurred during dehydration of the sample, in the preparation of the film over the Ge crystal. When we analyzed peptides cosedimented with LUVs, a significant association with the lipid membrane was observed. The L:P value in the pellet, estimated for each sample using eq 1 and reported in Table 4, was very similar to the correspondent ratio before centrifugation, suggesting that virtually each of peptides was associated with LUVs. A comparative analysis of the spectra recorded with or without LUVs indicated an unusual slight decrease in the level of α and β structure of each peptide upon interaction with membranes, with a concomitant increase in the level of disordered structure. The most significant changes were observed for distinctin and both peptide B-containing peptides; the α-helix content of these peptides in a membrane environment was reduced from 66−67 to 47−50%. However, their helical content in LUVs was 10% higher than that of peptide A or the peptide A−A homodimer.

From the 0° and 90° polarized spectra, we calculated the dichroic ratio of both the lipid acyl chains and the peptides bound to the membrane, obtaining the orientation of their structures with respect to the perpendicular to the plane of the membrane (*29*) (Table 5). Considering the average orientation of the lipid chains before and after incubation with peptides, we noticed a slight increment in the lipid tilt angle (γ_L) for distinctin and the peptide B−B homodimer (from 38° to 42°). This increment depended on peptide concentration; it was higher when the L:P value was ideal for the maximum formation of active pores on the membrane, i.e., $R_{\%} = 90\%$ for activity in an equivalent assay of calcein release. In this case, this value corresponded to 2.3 pores/LUV (*35*). These results were consistent with both the maximum binding and maximum insertion of peptides into the membrane (*36*).

On the other hand, the calculated average tilt angle of the α helices ($\gamma_{\alpha\perp}$) was lower at higher peptide concentrations (Table 5); in particular, the tilt angle of the distinctin α helix was 69° when $R_{\%} < 20\%$ (corresponding to 0.2 pore/LUV) and 55° when $R_{\%} = 90°$. These results suggested that in active pores, i.e., at higher $R_{\%}$ values, distinctin and peptide homodimers were more deeply inserted into the lipid core of the membrane. Whenever possible, the lipid tilt angle (γ_L) was used to calculate the relative orientation of the helices with respect to the lipid chains, providing tilt angles (γ_{α_L})

Table 1: MICs and MBCs (micromolar) of Distinctin Analogues Measured for Gram-Negative Bacteria[a]

	MIC[b]			MBC[b]		
	range	50%	90%	range	50%	90%
E. coli (10)						
A−B	0.73−11.68	5.84	11.68	1.46−23.36	11.68	23.36
A−A	0.79−12.67	6.33	12.67	1.58−25.33	12.67	25.33
B−B	0.68−10.84	5.42	10.84	1.35−21.68	10.84	21.67
A	1.58−25.33	6.33	25.33	3.16−50.65	25.33	50.65
B	1.35−21.67	5.42	21.67	2.71−43.34	10.83	43.34
polymyxin B	0.36−1.44	0.72	0.72	0.36−1.44	0.72	1.44
K. pneumoniae (10)						
A−B	0.73−23.37	5.84	23.37	1.46−23.36	11.68	23.36
A−A	0.79−25.33	6.33	25.33	1.58−25.33	12.67	25.33
B−B	0.68−21.67	5.42	21.68	1.35−21.67	10.84	21.67
A	1.58−50.65	12.66	25.32	3.16−50.65	25.32	50.65
B	1.35−43.34	10.83	21.67	2.71−43.34	10.83	43.34
polymyxin B	0.36−2.89	1.44	2.89	0.72−2.89	2.89	2.89
S. marcescens (10)						
A−B	1.46−46.73	11.68	23.36	1.46−46.73	11.68	46.73
A−A	1.58−50.67	12.67	25.33	3.17−50.67	12.67	50.67
B−B	1.35−43.35	10.84	21.67	1.35−43.35	10.84	43.35
A	3.16−101.30	25.32	50.65	3.16−101.30	25.32	101.30
B	2.71−43.34	21.67	43.34	2.71−86.68	21.67	86.68
polymyxin B	2.89−46.21	5.78	23.10	2.89−46.21	11.55	23.10
S. maltophilia (8)						
A−B	2.92−46.78			2.92−46.73		
A−A	3.17−50.67			3.17−50.67		
B−B	2.71−43.35			2.71−43.35		
A	6.33−101.30			6.33−101.30		
B	5.42−43.34			5.42−86.68		
polymyxin B	0.72−5.78			2.89−5.78		
A. baumannii (8)						
A−B	2.92−46.73			2.92−46.73		
A−A	3.17−50.67			3.17−50.67		
B−B	5.42−43.35			5.42−43.35		
A	6.33−101.30			12.67−101.30		
B	5.42−43.34			5.42−86.68		
polymyxin B	0.72−23.10			1.44−46.21		
P. aeruginosa (10)						
A−B	2.92−46.73	23.37	23.37	2.92−46.73	23.37	46.73
A−A	3.17−50.67	25.33	50.67	3.17−50.67	25.33	50.67
B−B	5.42−43.35	21.68	21.68	5.42−43.35	21.68	43.35
A	6.33−101.30	50.65	101.30	12.67−101.30	50.65	101.30
B	5.42−86.68	43.34	43.34	5.42−86.68	43.34	86.68
polymyxin B	0.36−5.78	1.44	2.89	0.72−11.55	1.44	5.78

[a] The number of isolates assayed for each microorganism is reported in parentheses. [b] The terms 50% and 90% stand for MICs (or MBCs) at which 50% and 90% of the isolates tested were inhibited (or killed), respectively.

of 57°, 77°, and 78° for the averaged α helix of the A−B, A−A, and B−B peptides, respectively.

^{31}P NMR Experiments. To better describe the interaction of distinctin with membranes, we studied the effect of this peptide on the bilayer structure of 1:1 POPC/DOPA multilamellar vesicles (MLVs). ^{31}P NMR was chosen for the study of the eventual peptide-induced change in lipid organization, i.e., from lamellar to isotropic phase, generally associated with membrane disruption. MLVs were used because, even at a high temperature, they show a clear predominance of the broad asymmetric signal in the ^{31}P NMR spectrum (with a low-field shoulder) (Figure 2 of the Supporting Information, inset) (*37, 38*). Changes in the overall chemical shift anisotropy (CSA) width, reflecting the structural or dynamic response of the lipid headgroups (indicative of lateral domain formation), were used to reveal lipid−peptide interactions. In pure 1:1 POPC/DOPA MLVs, the occurrence of two clear signals associated with the magnetically nonequivalent P nuclei of DOPA and POPC demonstrated the occurrence of the pure lamellar phase (Figure 2 of the Supporting Information, top panel). A chemical shift for the intense high-field spectrum edges (corresponding to lipid components whose normal bilayer axis is perpendicular to the magnetic field) was measured at δ −12.2 and −14.4 for DOPA and POPC, respectively (*39*). Since the individual spectral contribution of these lipids cannot be resolved by wide-line ^{31}P NMR spectroscopy, only an overall CSA value of 42 ppm was estimated.

The ^{31}P NMR wide-line spectrum of POPC/DOPA MLVs containing distinctin (L:P = 50:1) showed no deviation from the powder distribution (Figure 2 of the Supporting Information, bottom panel), indicating that the lipid system remained in the liquid crystalline lamellar phase. No isotropic peaks were detected after the addition of significant peptide amounts (data not shown). This finding ruled out not only a macroscopic detergent-like action of distinctin on the bilayer structure, in agreement with data reported previously (*16*) and above and dynamic light scattering measurements (not shown), but also the induction of "honeycomb structures" (*40*). This behavior was observed also at higher temperatures (Figure 5). Even though the presence of distinctin did not induce formation of nonlamellar phases, some reliable changes were observed in the spectrum. In fact, downfield effects of ∼2 (DOPA) and ∼0.5 ppm (DOPC) were observed

Table 2: MICs and MBCs (micromolar) of Distinctin Analogues Measured for Gram-Positive Bacteria[a]

	MIC[b]			MBC[b]		
	range	50%	90%	range	50%	90%
MS *S. aureus* (10)						
A−B	0.73−23.36	5.84	23.36	1.46−23.36	11.68	23.36
A−A	0.79−25.33	6.33	25.33	1.58−25.33	12.67	25.33
B−B	0.68−21.68	5.42	21.68	1.35−21.68	10.84	21.68
A	1.58−50.65	12.66	50.65	3.16−50.65	12.66	50.65
B	1.35−43.34	10.83	43.34	2.71−43.34	10.83	43.34
MR *S. aureus* (10)						
A−B	0.73−23.36	5.84	23.36	1.46−23.36	11.68	23.36
A−A	0.79−25.33	6.33	25.33	1.58−25.33	12.67	25.33
B−B	0.68−21.68	5.42	21.68	1.35−21.68	10.84	21.68
A	1.58−50.65	12.66	50.65	3.16−50.65	25.32	50.65
B	1.35−43.34	10.83	43.34	2.71−43.34	21.67	43.34
S. pneumoniae (10)						
A−B	0.73−23.36	5.84	11.68	0.73−23.36	11.68	23.36
A−A	0.79−25.33	6.33	12.67	1.58−25.33	12.67	25.33
B−B	0.68−21.68	5.42	10.84	0.68−21.68	10.84	21.68
A	1.58−50.65	12.66	25.32	3.16−50.65	12.66	50.65
B	1.35−43.34	10.83	21.67	2.71−43.34	10.83	43.34
E. faecium (5)						
A−B	2.92−46.73			2.92−46.73		
A−A	3.17−50.67			3.17−50.67		
B−B	2.71−43.35			2.71−43.35		
A	6.33−101.30			6.33−101.30		
B	5.42−43.34			5.42−86.68		
E. faecalis (10)						
A−B	0.73−23.36	11.68	23.37	1.46−23.36	23.37	23.37
A−A	0.79−25.33	12.67	25.33	1.58−25.33	25.33	25.33
B−B	0.68−21.68	10.84	21.68	1.35−21.68	21.68	21.68
A	1.58−50.65	25.32	50.65	3.16−50.65	50.65	50.65
B	1.35−43.34	21.67	43.34	2.71−21.67	21.67	21.67

[a] The number of isolates assayed for each microorganism is reported in parentheses. [b] The terms 50% and 90% are MICs (or MBCs) at which 50% and 90% of the isolates tested were inhibited (or killed), respectively.

Table 3: Permeabilizing Activities of Distinctin and Peptide Analogues on Vesicles with Different Lipid Compositions[a]

	C_{50} (μM)				
LUV100	A−B	A−A	B−B	A[b]	B[b]
asolectin	<20%[c]	<20%[c]	<30%[e]	<20%[c]	<20%[c]
POPC	na[d]	na[d]	na[d]	na[d]	na[d]
POPC/Ch	na[d]	na[d]	na[d]	na[d]	na[d]
POPC/Ch/SM	na[d]	na[d]	na[d]	na[d]	na[d]
POPC/SM	na[d]	na[d]	na[d]	na[d]	na[d]
POPC/DOPE	na[d]	na[d]	na[d]	na[d]	na[d]
POPC/DOPG	0.30	0.50	0.07	<20%[c]	<30%[e]
POPC/DOPA	0.10	0.17	0.19	<20%[c]	0.82
POPC/PS	0.09	0.37	0.06	<20%[c]	0.72
POPC/PI	0.04	0.28	0.02	<20%[c]	0.25

[a] Lipid mixtures reported in the text are given on an equimolar molar basis. The permeabilizing assay was performed as described in Experimental Procedures. [b] In the presence of DTT (20:1 DTT/peptide). [c] Determining a 20% release of calcein at a concentration of 1 μM. [d] Nonactive at a concentration of up to 1 μM. [e] Determining a 30% release of calcein at a concentration of 1 μM.

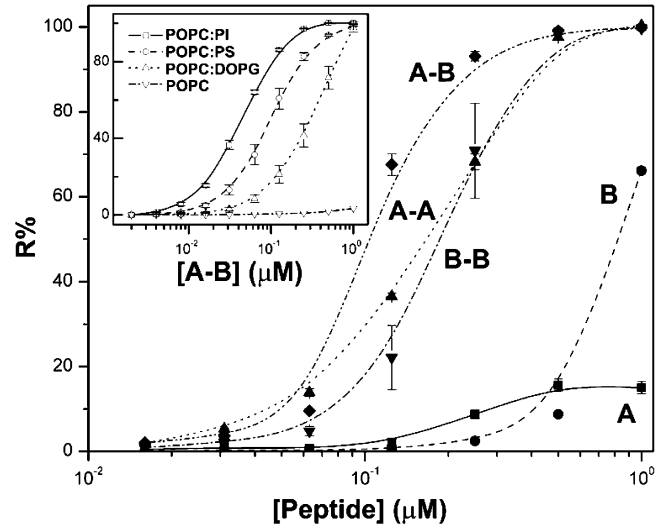

FIGURE 4: Dose dependence permeabilizing activity of distinctin and peptide analogues on liposomes with different lipid compositions. Calcein-loaded liposomes (1:1 POPC/DOPA) were exposed to different peptide concentrations, and the percentage of calcein released after 45 min is reported: distinctin (◆), peptide A (■), peptide B (●), peptide A−A homodimer (▲), and peptide B−B homodimer (▼). The inset shows the activity of distinctin on liposomes having different lipid compositions (as indicated in the figure). The lipid concentration in both assays was 6−8 μM.

for their corresponding intense high-field edges, indicating a strong electrostatic interaction between distinctin and DOPA headgroups. Moreover, although the widths of the spectra obtained for the lipid/peptide mixture were found to be only slightly smaller than those observed for the lipid alone (measured ΔCSA $\sim$ 2.0 ppm), the corresponding line shapes showed differences that could be attributed to a redistribution of the signal intensities between upfield peaks and the low-field shoulder. With an increase in temperature, a clear predominance of the broad asymmetric ^{31}P NMR spectra (with a low-field shoulder), typical of the lamellar phase, was observed together with a small decrease in the overall CSA (Figure 5). This behavior exhibited strong similarities with that reported for the barrel-stave-forming peptide alamethicin in 1,2-dimyristoyl-*sn*-glycero-3-phosphocholine (*41, 42*). In this case, ^{31}P NMR data were interpreted as evidence that the peptide leads to slight changes in the orientation of the headgroups, without changing the conformation of the lipid side chains.

Table 4: FTIR Spectroscopic Determination of the Secondary Structure of Distinctin and Peptide Analogues[a]

system	peptide	secondary structure (%)[b] α	β	r	% βAgg[c]	L:P	$R_{\%}$[d]
without LUVs	A−B	67	24	9	−	−	−
	A−A	43	38	19	−	−	−
	B−B	66	24	10	−	−	−
	A	45	38	17	29	−	−
	B	66	21	13	−	−	−
with LUVs	A−B	50	23	27	−	50	90
	A−A	39	36	25	−	25	90
	B−B	49	20	31	−	35	90
	A	40	35	25	−	60	<20
	B	47	20	33	−	50	<20

[a] Measurements were performed on dried samples from 10 mM Hepes (pH 7.4) or on 1:1 POPC/DOPA LUVs prepared in 10 mM Hepes (pH 7.4), as described in Experimental Procedures. [b] Percentages refer to the nonaggregated part: α, α helix; β, β structure; r, random coil. Errors are ±5%. [c] Total aggregated peptide calculated from the relative areas of the corresponding Gaussian bands (Agg_I and Agg_{II} in Figure 1 of the Supporting Information). [d] Percentage of activity at that L:P in calcein release assays.

Table 5: Orientations of the Lipid Acyl Chains in the Membrane and of the Peptide Analogues Inserted into It

sample	$R_{\%}$[a]	γ_L (deg)[b]	$\gamma_{\alpha\perp}$ (deg)[c]	$\gamma_{\alpha L}$ (deg)[d]
only LUVs	−	38	−	−
LUVs with A	<20	36	81	90
LUVs with B		36	90	90
LUVs with A−A		42	69	90
LUVs with B−B		39	74	90
LUVs with A−B		36	69	90
LUVs with A	90	−	−	−
LUVs with B		−	−	−
LUVs with A−A		38	64	77
LUVs with B−B		41	64	78
LUVs with A−B		42	55	57

[a] Percentage of activity in calcein release assays at the same L:P: when $R_{\%} < 20\%$, a prepore structure is favored with most of peptide molecules oriented parallel to the membrane surface; on the other hand, at higher peptides concentrations where $R_{\%} = 90\%$, the maximum formation of active pores on the membrane is reached, with peptides molecules probably inserted into the lipid core. [b] Average angle between the direction of the lipid molecular axis and the perpendicular to the crystal plane (i.e., the membrane plane). [c] Average angle between the direction of the helix molecular axis and the perpendicular to the crystal plane (i.e., the membrane plane). [d] Average angle between the direction of the helix molecular axis and that of the lipid chains.

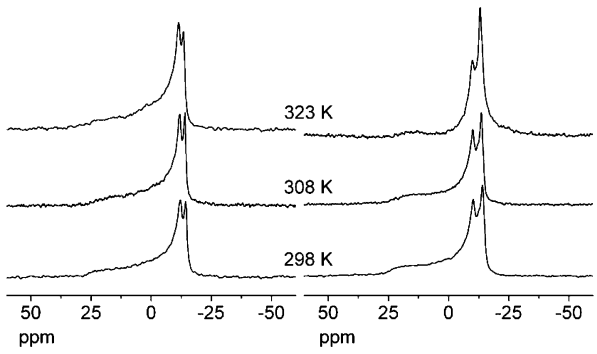

FIGURE 5: ^{31}P NMR measurements. ^{31}P NMR spectra (90:10 H_2O/D_2O) recorded at different temperatures (298, 308, and 323 K) of 1:1 POPC/DOPA MLVs [30 mM total lipid, 10 mM Hepes, and 100 mM NaCl (pH 7.0)], without (left) and with (right) 0.6 mM distinctin, at a lipid:peptide molar ratio of 50:1.

Molecular Modeling. Although the possible coexistence of porelike structures and different states of adsorbed peptide molecules may in principle affect the interpretation of experimental data in terms of atomic structural parameters, preliminary MD calculations on single and multiple (but not pore-aggregated) molecules adsorbed on POPC/DOPA bilayers showed that distinctin seems to assume prevalently either (i) a monomeric structure in which only a single helical chain is half-embedded in the bilayer, almost parallel to its surface, while the other chain sweeps in the aqueous medium or (ii) dimeric/oligomeric prepore arrangements, where two or more helical chains from different monomers are inserted into the bilayer, forming direct and water-mediated polar interactions with each other, with the other chain of each monomer adsorbed parallel to the lipid membrane. In both cases, the calculated average helix−lipid angles were not far from the measured values (Table 5). Consequently, at the concentrations at which porelike structures also contribute to the overall peptide distribution, their average helix−lipid angles cannot deviate appreciably from the experimental values reported in Table 5.

On the basis of previous evidence showing that distinctin is able to form pores within membranes, several models of polypeptide pores were built up in 1:1 POPC/DOPA bilayers by varying peptide stoichiometry, inner pore diameter, relative interhelix orientation, and relative helical assembly bilayer orientation. In particular, pores containing from four to six distinctin molecules were built up, with starting internal diameters ranging from 17.5 to 25 Å. Three possible relative helical arrangements, compatible with observed average helix−bilayer plane angles (Table 5) and with the possibility of building similar models also for A−A and B−B peptides (Tables 1–5), were tested. In model I, A helices are perpendicular to the bilayer normal, while B helices are inserted into the bilayer, forming the walls of the pore (Figure 6A,D). Model II is the same as model I, but with swapped A and B helices (Figure 6B,E). In model III, helices A and B are both inserted into the bilayer and contribute to formation of the pore walls by interacting with adjacent distinctin molecules (Figure 6C,F). The tilt angle of the inserted helix in models I and II and the overall helical arrangement in model III was chosen to reproduce the average value of the helix−bilayer plane angle reported in Table 5.

The final MD models were analyzed in terms of the inner diameter of the pore, the average degree of helicity, the average helical−bilayer plane angle, and the average lipid chain−bilayer plane angle. The models obtained from the three tested molecular arrangements were all potentially compatible with measured parameters (Tables 3–5), although the minimal number of distinctin molecules providing a pore diameter that allows a free diffusion of calcein molecule varied from four (for model III) to five or six (for models I and II). In all models, the amphipatic nature of the pore was maintained and both intra- and intermolecular stabilizing interhelical interactions were observed. In addition, in agreement with observed variations in lipid chain−bilayer plane average angle values (Table 5), a different kind of funnel-like distortion of the lipid distribution at both ends of the pore was detected. This distortion was associated with a reduction of the bilayer thickness around the pore, whose extension and amount differed among the three models (Figure 6G−I). If pentameric pores are considered, the decrease in thickness for model III extended for 20 Å from the outer peptide channel walls, with a maximum value of 7

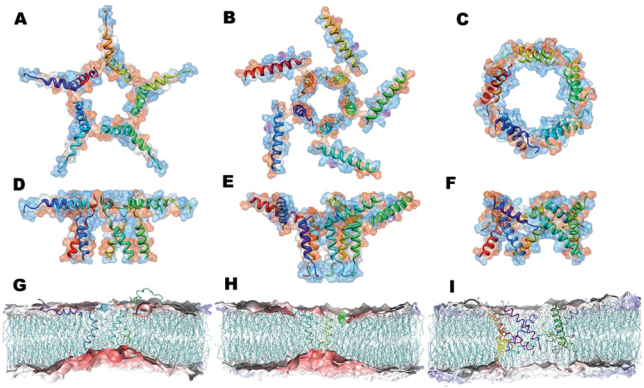

FIGURE 6: Modeling of distinctin pores. The three different model families described in the text are shown for distinctin pentamers. Models I (panels A and D), II (panels B and E), and III (panels C and F) are viewed along directions perpendicular (panels A−C) and parallel (panels D−F) to the lipid membrane plane, using a ribbon representation with a "rainbow" coloring scheme (i.e., different colors from red to violet for each peptide chain). Transparent accessible surfaces, painted according to residue hydrophobicity scale, ranging from blue (for hydrophilic) to red (for hydrophobic), are also shown. Panels G−I illustrate the final lipid bilayer deformations observed in MD simulations of the three pentamers. To represent bilayer external surfaces, a solvent-accessible surface with a probe radius of 6.5 Å was depicted for lipid P and N atoms. This surface was painted with a color scale ranging from red to blue, for increasing distances from the membrane center. Peptide chains are shown as thin tubes, painted according the rainbow scheme, while bonds involving lipid heavy atoms are depicted as cylinders colored according to atom type (cyan for C, red for O, blue for N, and pink for P). Only the posterior half of the simulated system, without water and counterions, is shown for the sake of clarity.

Å on each side and an almost symmetrical distribution of the two bilayer surfaces. For models I and II, the decrease was substantially less symmetrical between the two surfaces, being more pronounced on the surface opposed to the peptide chain perpendicular to the bilayer normal (15 Å in models I and II, where it extends for 30−35 Å from the outer peptide channel wall), leading in both cases to an overall curvature of the lipid bilayer.

Models I and II exhibited larger fluctuations and lower average values in helical contents in comparison with distinctin structure in water than model III. Partial dynamic helix unfolding was present around the disulfide bond and at the N-terminus of both peptide chains (Figure 6). In particular, helices inserted perpendicularly into the membrane tended to unfold prevalently their C-terminus (model I) or N-terminus (model II) to increase the overall depth of penetration into the bilayer, optimizing polar interactions with lipid polar heads. On the other hand, the degree of unfolding for the N-terminus of helices parallel to the membrane surface followed the embedding of the helix into the bilayer, as the N-terminal group always tended to emerge from the lipid surface.

DISCUSSION

There is a growing body of evidence that the ability of antimicrobial peptides to structure and aggregate in solution before reaching the target membrane could also have a significant effect on both antimicrobial potency and selectivity with respect to host cells (*43, 44*). This tendency, driven by both ionic and hydrophobic interactions, has been identified as an important factor in the membranolytic activity of helical cathelicidin LL-37 and other β-sheet peptides (*45, 46*). In this respect, it is interesting to note that a growing number of antimicrobial peptides have been recently demonstrated to have hetero- and homodimeric structures stabilized by a single disulfide bond linking linear polypeptide chains, namely distinctin (*9*), dicynthaurin (*10*), halocidin (*11*), and cathelicidins CAP11 and PMAP36 (*12, 13*). Related antimicrobial compounds have also been synthesized by oxidation of linear Cys-containing peptide analogues deriving from magainin 2 (*47*), lentivirus envelope protein (*48*), and halocidin (*14*). Conformational studies with respect to monomeric derivatives proved that dimerization does not affect the intrinsic tendency of a peptide to adopt a helical conformation in membrane-mimicking environments (*9, 10, 13–16, 47*). Comparative assays with respect to monomeric derivatives performed on Gram-positive and -negative bacteria provided controversial data. In fact, dimerization in CAP11, PMAP36, and dicynthaurin does not seem to affect peptide MIC values (*10, 12, 13*); in contrast, dimeric halocidin, lentivirus, and magainin peptides have shown a 4−20-fold increase in permeabilization and antimicrobial activity, marked at low peptide concentrations (*11, 14, 47, 48*). Whenever tested, dimeric peptides exhibited bacterial inactivation with kinetics faster than those of monomeric molecules (*11, 13, 47*). This tendency was associated with an increased density of positively charged amino acids for the peptide molecule, which seems to enhance binding to negatively charged bacterial membrane surfaces (*3, 34*).

To investigate the contribution of the distinct peptide chains and the C-terminal intermolecular disulfide on distinctin biochemical properties, different monomeric and homodimeric analogues were synthesized and comparatively evaluated with respect to the native molecule (Figure 1). Our results demonstrate that the simultaneous occurrence of distinct peptide chains linked by a disulfide bond is essential for the formation of the final distinctin quaternary structure in aqueous media. In fact, only the native heterodimeric peptide, but not the monomeric or homodimeric peptides, is able to aggregate in a stable noncovalent dimeric structure (Figure 2). This compact oligomeric form is responsible for the unique resistance of the native peptide to protease action; in fact, none of the monomeric and dimeric peptides resisted to proteolysis, except distinctin (Figure 3). This structural feature could be essential in determining a prolonged action of distinctin toward pathogens exerting resistance to other antimicrobial peptides by constitutive and/or inducible expression of proteases (*3*). In contrast, distinctin and monomeric and homodimeric analogues exhibited comparable antimicrobial activities against Gram-positive and -negative bacteria (Tables 1 and 2). In general, an only 2−3-fold increase in antimicrobial activity was observed for distinctin and homodimeric peptides with respect to monomeric ones. These findings were in line with the data determined for the other dimeric peptides mentioned above (*10–14, 47, 48*). Thus, the disulfide bond seems only to partly contribute to the killing effectiveness of distinctin against microorganisms. Relative antimicrobial activities of distinctin analogues paralleled well the leakage of calcein encapsulated into lipid vesicles (Table 3 and Figure 4). These

results, the L:P values determined during liposome preparation, and the ^{31}P NMR data on specific MLVs (Figure 5 and Figure 2 of the Supporting Information) confirmed the good propensity of distinctin peptides to associate with lipid vesicles. These experiments definitively demonstrated that microbial membranes are the main target of distinctin activity (*9, 16*). The permeabilization measurements reported here demonstrate a stronger activity of distinctin toward liposomes containing negatively charged lipids (Table 3 and Figure 4). This phenomenon, evident for dimeric or chain B-containing species, was associated with the number of positively charged amino acids on each peptide molecule (net charges of +7, +6, +8, +3, and +4 for distinctin, A−A, B−B, A, and B peptide, respectively), which favor initial electrostatic attraction to negatively charged headgroups of lipid membranes (*3*). A further confirmation of this hypothesis derived from the down-field effects of ∼2 and ∼0.5 ppm for the intense high-field edges of DOPA and DOPC, observed in ^{31}P NMR experiments after addition of distinctin to MLVs (Figure 5 and Figure 2 of the Supporting Information).

ATR-FTIR spectroscopy measurements provided information about the secondary structure of each peptide as a pure component or as adsorbed to 1:1 POPC/DOPA LUVs (Table 4). Frequency component analysis confirmed previous data for distinctin in aqueous solution and indicated that chain B-containing peptides also adopted a helical conformation in this medium. A comparative analysis of the spectra suggested an unusual slight decrease in the secondary structure content of each peptide, passing into the lipid phase. Changes were observed for distinctin and all chain B-containing peptides. Induction of structured amphipatic helical conformers has been well documented during the phase transition of linear peptides having a random coil structure in water (*2–4*); an opposite phenomenon was observed in this case. Since distinctin and related analogues were shown to adopt a helical structure in aqueous media, these results were indicative of the occurrence of a peptide conformational rearrangement upon interaction with lipid membranes. For distinctin, this event is probably associated with the disassembly of the symmetrical full-parallel four-helix bundle structure present in aqueous media.

The calculated dichroic ratios of both the lipid acyl chains and the peptides bound to the membrane provided indications of the orientation of molecular structures with respect to the perpendicular to the plane of the membrane (Table 5). In the case of distinctin and the B−B homodimer, γ_L determinations suggested that the insertion of distinctin and some of its analogues caused a slight increase in the level of membrane disorder, which has been considered a typical behavior for a barrel-stave pore (*49*); this increment depended on peptide concentration. For the same reason and in agreement with previously published data for other peptides (*50*), the calculated $\gamma_{\alpha\perp}$ was lower at higher peptide concentrations, meaning that distinctin and peptide homodimer were more deeply inserted into the lipid core of the membrane under these conditions. In particular, the tilt angle of the averaged distinctin α helix was 69° when $R_{\%} < 20\%$ and 55° when $R_{\%} = 90°$. According to these data, we concluded that the orientation of the molecular averaged α helix in the lipid core depended on peptide nature and concentration. At higher concentrations, the peptides were more inserted into the membrane, with an orientation decreasing from A−B (the most immersed) to A−A and B−B. This concentration-dependent realignment of the helical axis with respect to the lipid bilayer resembles the behavior of other pore-forming peptides, namely, PGLa and magainins (*7, 51, 52*). Recently, a synergistic transmembrane alignment of the antimicrobial PGLs−magainin noncovalent heterodimer toward a pore structure has been reported (*53*). Further investigations will ascertain if the behavior of the distinctin covalent heterodimer in membranes during pore formation resembles that occurring for the PGLs−magainin noncovalent oligomer.

In agreement with FTIR data, ^{31}P NMR experiments with MLVs reported in Figure 5 and Figure 2 of the Supporting Information indicate that, after addition of distinctin, the lipid system does not present nonlamellar phases, otherwise occurring with peptides acting with a carpet-like mechanism. These results confirmed previous evidence of the ability of distinctin to form supramolecular channel-forming peptide structures. In fact, macroscopic and single-channel conductance experiments demonstrated for distinctin a multistate behavior, with a geometrical progression of increments similar to that measured for a barrel-stave-forming peptide, alamethicin (*16*). Although associated with smaller CSA width differences (2.0 vs 5 ppm), the line shape changes of the ^{31}P NMR spectra recorded at different temperatures presented characteristics similar to those already reported for alamethicin (*41, 42*). This redistribution of the signal intensities between up-field peaks and the low-field shoulder was attributed to small spin−spin relaxation time T_2 changes of the ^{31}P nuclei.

Three different model families of transmembrane peptide supramolecular pore complexes compatible with experimental measurements were obtained with MD simulations (Figure 6), which differ for the relative arrangement of the two helices and/or their orientation inside the membrane. For each family, pores formed from four to six monomers were simulated. In agreement with the relative length of the helical portions observed in the aqueous (*16*) or membrane-like environment (Figure 1 and Table 4), they presented the B helices as being inserted into the membrane but differed for the relative embedding of the A helices into the lipid bilayer and their direct participation in the ion-channel pack. The minimal number of distinctin molecules providing a pore diameter compatible with calcein diffusion varied from four (model III) to five or six (models I and II). In all models, the amphipathic nature of the pore was maintained and both intra- and intermolecular stabilizing interhelical interactions were observed. Different kinds of funnel-like distortion of the lipid distribution at both ends of the pore were detected. The substantial agreement of all models with measured structural parameters (Tables 3–5) presently prevents us from suggesting a unique pore model, the definitive proposition of which will require both further experimental data, such as estimates for exact pore size and/or stoichiometry, and more intensive computational efforts. However, on the basis of the observed decrease in helical content on going from water to a membrane environment, and variations of helix tilt angles with concentration, a preference for distinctin models I and II could be inferred.

In conclusion, the various biophysical experiments performed in membrane-mimicking systems here presented

nicely correlate with proposed microbial membranes as the main target of distinctin activity. The experimental output recorded so far for the distinctin mechanism of insertion into membranes is compatible with a barrel-stave pore. Future studies, including solid-state NMR analysis of ^{15}N-labeled peptides in a lipid bilayer, will definitively elucidate the structure of the distinctin−lipid supramolecular pore complex, providing a molecular rationale for the antimicrobial action of a molecule with promising biomedical applications (*54*). These investigations will better clarify whether limit mechanisms already described for linear peptides, such as the barrel-stave or toroid wormhole models (*3, 4, 22–24*), may be suitable for description of membrane permeabilization by covalent heterodimeric peptides or other intermediate and more complex pictures have to be considered.

SUPPORTING INFORMATION AVAILABLE

Further experimental details of NMR experiments and molecular modeling, infrared attenuated total reflection spectra of distinctin and peptide analogues (Figure 1), and ^{31}P NMR measurements (Figure 2). This material is available free of charge via the Internet at http://pubs.acs.org.

REFERENCES

1. Barra, D., and Simmaco, M. (1995) Amphibian skin: a promising resource for antimicrobial peptides. *Trends Biotechnol. 13*, 205–209.
2. Zasloff, M. (2002) Antimicrobial peptides of multicellular organisms. *Nature 415*, 389–395.
3. Yeaman, M. R., and Yount, N. Y. (2003) Mechanisms of antimicrobial peptide action and resistence. *Pharmacol. Rev. 55*, 27–55.
4. Oren, Z., and Shai, Y. (1999) Mode of action of linear amphipathic α-helical antimicrobial peptides. *Biopolymers 47*, 451–463.
5. Lequin, O., Ladram, A., Chabbert, L., Bruston, F., Convert, O., Vanhoye, D., Chassaing, G., Nicolas, P., and Amiche, M. (2006) Dermaseptin S9, an α-helical antimicrobial peptide with a hydrophobic core and cationic termini. *Biochemistry 45*, 468–480.
6. Vignal, E., Chavanieu, A., Roch, P., Chiche, L., Grassy, G., Calas, B., and Aumelas, A. (1998) Solution structure of the antimicrobial peptide ranalexin and a study of its interaction with perdeuterated dodecylphosphocholine micelles. *Eur. J. Biochem. 253*, 221–228.
7. Bechinger, B., Zasloff, M., and Opella, S. J. (1998) Structure and dynamics of the antibiotic peptide PGLa in membranes by solution and solid-state nuclear magnetic resonance spectroscopy. *Biophys. J. 74*, 981–987.
8. Park, S. H., Kim, Y. K., Park, J. W., Lee, B., and Lee, B. J. (2000) Solution structure of the antimicrobial peptide gaegurin 4 by ^{1}H and ^{15}N NMR spectroscopy. *Eur. J. Biochem. 267*, 2695–2704.
9. Batista, C. V., Scaloni, A., Rigden, D. J., Silva, L. R., Rodrigues Romero, A., Dukor, R., Sebben, A., Talamo, F., and Bloch, C. (2001) A novel heterodimeric antimicrobial peptide from the tree-frog *Phyllomedusa distincta*. *FEBS Lett. 494*, 85–89.
10. Lee, I. H., Lee, Y. S., Kim, C. H., Kim, C. R., Hong, T., Menzel, L., Boo, L. M., Pohl, J., Sherman, M. A., Waring, A., and Lehrer, R. I. (2001) Dicynthaurin: an antimicrobial peptide from hemocytes of the solitary tunicate *Halocynthia aurantium*. *Biochim. Biophys. Acta 1527*, 141–148.
11. Jang, W. S., Kim, K. N., Lee, Y. S., Nam, M. H., and Lee, I. H. (2002) Halocidin: A new antimicrobial peptide from hemocytes of the solitary tunicate *Halocynthia aurantium*. *FEBS Lett. 521*, 81–86.
12. Yomogida, S., Nagaoka, I., and Yamashita, T. (1996) Purification of the 11- and 5-kDa antibacterial polypeptides from guinea pig neutrophils. *Arch. Biochem. Biophys. 328*, 219–226.
13. Scocchi, M., Zelezetsky, I., Benincasa, M., Gennaro, R., Mazzoli, A., and Tossi, A. (2005) Structural aspects and biological properties of the cathelicidin PMAP-36. *FEBS J. 272*, 4398–4406.
14. Jang, W. S., Kim, C. H., Kim, K. N., Park, S. Y., Lee, J. H., Son, S. M., and Lee, I. H. (2003) Biological activities of synthetic analogs of halocidin, an antimicrobial peptide from the tunicate *Halocynthia aurantium*. *Antimicrob. Agents Chemother. 47*, 2481–2486.
15. Okuda, D., Yomogida, S., Tamura, H., and Nagaoka, I. (2006) Determination of the antibacterial and lipopolysaccharide-neutralizing regions of guinea pig neutrophil cathelicidin peptide CAP11. *Antimicrob. Agents Chemother. 50*, 2602–2607.
16. Raimondo, D., Andreotti, G., Saint, N., Amodeo, P., Renzone, G., Sanseverino, M., Zocchi, I., Molle, G., Motta, A., and Scaloni, A. (2005) A folding-dependent mechanism of antimicrobial peptide resistance to degradation unveiled by solution structure of distinctin. *Proc. Natl. Acad. Sci. U.S.A. 102*, 6309–6314.
17. Mangoni, M. L., Saugar, J. M., Dellisanti, M., Barra, D., Simmaco, M., and Rivas, L. (2005) Temporins, small antimicrobial peptides with leishmanicidal activity. *J. Biol. Chem. 280*, 984–990.
18. Brand, G. D., Leite, J. R., Silva, L. P., Albuquerque, S., Prates, M. V., Azevedo, R. B., Carregaro, V., Silva, J. S., Sa, V. C., Brandao, R. A., and Bloch, C. (2002) Dermaseptins from *Phyllomedusa oreades* and *Phyllomedusa distincta*: anti-*Trypanosoma cruzi* activity without cytotoxicity to mammalian cells. *J. Biol. Chem. 277*, 49332–49340.
19. Ohsaki, Y., Gazdar, A. F., Chen, H. C., and Johnson, B. E. (1992) Antitumor activity of magainin analogues against human lung cancer cell lines. *Cancer Res. 52*, 3534–3538.
20. Cruciani, R. A., Barker, J. L., Zasloff, M., Chen, H. C., and Colamonici, O. (1991) Antibiotic magainins exert cytolytic activity against transformed cell lines through channel formation. *Proc. Natl. Acad. Sci. U.S.A. 88*, 3792–3796.
21. Zairi, A., Serres, C., Tangy, F., Jouannet, P., and Hani, K. (2008) In vitro spermicidal activity of peptides from amphibian skin: dermaseptin S4 and derivatives. *Bioorg. Med. Chem. 16*, 266–275.
22. Shai, Y. (1999) Mechanism of the binding, insertion and destabilization of phospholipid bilayer membranes by α-helical antimicrobial and cell non-selective membrane-lytic peptides. *Biochim. Biophys. Acta 1462*, 55–70.
23. Matsuzaki, K. (1999) Why and how are peptide-lipid interactions utilized for self-defense? Magainins and tachyplesins as archetypes. *Biochim. Biophys. Acta 1462*, 1–10.
24. Yang, L., Weiss, T. M., Lehrer, R. I., and Huang, H. W. (2000) Crystallization of antimicrobial pores in membranes: Magainin and protegrin. *Biophys. J. 79*, 2002–2009.
25. Clinical and Laboratory Standards Institute (2003) Methods for dilution antimicrobial susceptibility tests for bacteria that grow aerobically, Approved Standard M7-A6, Villanova, PA.
26. Scaloni, A., Dalla Serra, M., Amodeo, P., Mannina, L., Vitale, R. M., Segre, A. L., Cruciani, O., Lodovichetti, F., Greco, M. L., Fiore, A., Gallo, M., D'Ambrosio, C., Coraiola, M., Menestrina, G., Graniti, A., and Fogliano, V. (2004) Structure, conformation and biological activity of a novel lipodepsipeptide from *Pseudomonas corrugata*: cormycin A. *Biochem. J. 384*, 25–36.
27. Coraiola, M., Lo Cantore, P., Lazzaroni, S., Evidente, A., Iacobellis, N. S., and Dalla Serra, M. (2006) WLIP and tolaasin I, lipodepsipeptides from *Pseudomonas reactans* and *Pseudomonas tolaasii*, permeabilise model membranes. *Biochim. Biophys. Acta 1758*, 1713–1722.
28. Alvarez, C., Dalla Serra, M., Potrich, C., Bernhart, I., Tejuca, M., Martinez, D., Pazos, I. F., Lanio, M. E., and Menestrina, G. (2001) Effects of lipid composition on membrane permeabilization by Sticholysin I and II, two cytolysins of the sea anemone *Stichodactyla helianthus*. *Biophys. J. 80*, 2761–2774.
29. Menestrina, G. (2000) Use of Fourier-transformed infrared spectroscopy (FTIR) for secondary structure determination of staphylococcal pore-forming toxins. In *Bacterial toxins, methods and protocols* (Holst, O., Ed.) pp 115−132, Humana Press, Totowa, NJ.
30. Goormaghtigh, E., Raussens, V., and Ruysschaert, J. M. (1999) Attenuated total reflection infrared spectroscopy of proteins and lipids in biological membranes. *Biochim. Biophys. Acta 1422*, 105–185.
31. Susi, H., and Byler, D. M. (1986) Resolution enhanced Fourier transform infrared spectroscopy of enzymes. *Methods Enzymol. 130*, 290–311.
32. Gordon, L. M., Mobley, P. W., Pilpa, R., Sherman, M. A., and Waring, A. J. (2002) Conformational mapping of the N-terminal peptide of HIV-1 gp41 in membrane environments using ^{13}C-enhanced Fourier transform IR spectroscopy. *Biochim. Biophys. Acta 1559*, 96–120.
33. Fontana, A., Polverino de Laureto, P., De Filippis, V., Scaramella, E., and Zambonin, M. (1997) *Folding Des. 2*, R17–R26.

34. Shai, Y. (2002) Mode of action of membrane active antimicrobial peptides. *Biopolymers 66*, 236–248.
35. Schwarz, G., and Robert, C. H. (1990) Pore formation kinetics in membranes, determined from the release of marker molecules out of liposomes or cells. *Biophys. J. 58*, 577–583.
36. Huang, H. W. (2006) Molecular mechanism of antimicrobial peptides: the origin of cooperativity. *Biochim. Biophys. Acta 1758*, 1292–1302.
37. Liu, F., Lewis, R. N. A. H., Hodges, R. S., and McElhaney, R. N. (2001) A differential scanning calorimetric and ^{31}P NMR spectroscopic study of the effect of transmembrane α-helical peptides on the lamellar-reversed hexagonal phase transition of phosphatidylethanolamine model membranes. *Biochemistry 40*, 760–768.
38. Hori, Y., Demura, M., Niidome, T., Aoyagi, H., and Asakura, T. (1999) Orientational behavior of phospholipid membranes with mastoparan studied by ^{31}P solid state NMR. *FEBS Lett. 455*, 228–232.
39. Dennis, E. A., and Plueckthun, A. (1984) ^{31}P NMR of phospholipids in micelles. In *^{31}P NMR, Principles and Applications* (Gorenstein, D. G., Ed.) pp 423−446, Academic Press, New York.
40. Anderluh, G., Dalla Serra, M., Viero, G., Guella, G., Macek, P., and Menestrina, G. (2003) Pore formation by equinatoxin II, an eukaryotic protein toxin, occurs by induction of non-lamellar lipid structures. *J. Biol. Chem. 278*, 45216–45223.
41. Banerjee, U., Zidovetzki, R., Birge, R. R., and Chan, S. I. (1985) Interaction of alamethicin with lecithin bilayers: a ^{31}P and ^{2}H NMR study. *Biochemistry 24*, 7621–7627.
42. Bechinger, B., Skladnev, D. A., Ogrel, A., Li, X., Rogozhkina, E. V., Ovchinnikova, T. V., O'Neil, J. D., and Raap, J. (2001) ^{15}N and ^{31}P solid-state NMR investigations on the orientation of zervamicin II and alamethicin in phosphatidylcholine membranes. *Biochemistry 40*, 9428–9437.
43. Loll, P. J., Miller, R., Weeks, C. M., and Axelsen, P. H. (1998) A ligand-mediated dimerization mode for vancomycin. *Chem. Biol. 5*, 293–298.
44. Hornef, M. W., Pütsep, K., Karlsson, J., Refai, E., and Andersson, M. (2004) Increased diversity of intestinal antimicrobial peptides by covalent dimer formation. *Nat. Immunol. 5*, 836–843.
45. Oren, Z., Lerman, J. C., Gudmundsson, G. H., Agerberth, B., and Shai, Y. (1999) Structure and organization of the human antimicrobial peptide LL-37 in phospholipid membranes: Relevance to the molecular basis for its non-cell-selective activity. *Biochem. J. 341*, 501–513.
46. Schibli, D. J., Hunter, H. N., Aseyev, V., Starner, T. D., Wiencek, J. M., Jr., Tack, B. F., and Vogel, H. J. (2002) The solution structures of the human β-defensins lead to a better understanding of the potent bactericidal activity of HBD3 against *Staphylococcus aureus*. *J. Biol. Chem. 277*, 8279–8289.
47. Dempsey, C. E., Ueno, S., and Avison, M. B. (2003) Enhanced membrane permeabilization and antibacterial activity of a disulfide-dimerized magainin analogue. *Biochemistry 42*, 402–409.
48. Tencza, S. B., Creighton, D. J., Yuan, T., Vogel, H. J., Montelaro, R. C., and Mietzner, T. A. (1999) Lentivirus-derived antimicrobial peptides: increased potency by sequence engineering and dimerization. *J. Antimicrob. Chemother. 44*, 33–41.
49. Yang, L., Harroun, T. A., Weiss, T. M., Ding, L., and Huang, H. W. (2001) Barrel-stave model or toroidal model? A case study on melittin pores. *Biophys. J. 81*, 1475–1485.
50. Lee, M. T., Chen, F. Y., and Huang, H. W. (2004) Energetics of pore formation induced by membrane active peptides. *Biochemistry 43*, 3590–3599.
51. Glaser, R. W., Sachse, C., Dürr, U. H., Wadhwani, P., and Ulrich, A. S. (2004) Orientation of the antimicrobial peptide PGLa in lipid membranes determined from ^{19}F-NMR dipolar couplings of 4-CF3-phenylglycine labels. *J. Magn. Reson. 168*, 153–163.
52. Tremouilhac, P., Strandberg, E., Wadhwani, P., and Ulrich, A. S. (2006) Conditions affecting the re-alignment of the antimicrobial peptide PGLa in membranes as monitored by solid state ^{2}H-NMR. *Biochim. Biophys. Acta 1758*, 1330–1342.
53. Tremouilhac, P., Strandberg, E., Wadhwani, P., and Ulrich, A. S. (2006) Synergistic transmembrane alignment of the antimicrobial heterodimer PGLa/magainin. *J. Biol. Chem. 281*, 32089–32094.
54. Giacometti, A., Cirioni, O., Ghiselli, R., Orlando, F., Silvestri, C., Renzone, G., Testa, I., Mocchegiani, F., Della Vittoria, A., Saba, V., Scaloni, A., and Scalise, G. (2007) Distinctin improves the efficacies of glycopeptides and betalactams against staphylococcal Biofilm in an experimental model of central venous catheter infection. *J. Biomed. Mater. Res., Part A 81*, 233–239.

BI800616K